HHS Public Access

Author manuscript

MAGMA. Author manuscript; available in PMC 2018 April 01.

Published in final edited form as:

MAGMA. 2018 April ; 31(2): 295–307. doi:10.1007/s10334-017-0646-8.

Highly Accelerated Intracranial 4D Flow MRI: Evaluation on Healthy Volunteers and Patients with Intracranial Aneurysms

Jing Liu[1,*], **Louise Koskas**[1], **Farshid Faraji**[1], **Evan Kao**[1], **Yan Wang**[1], **Henrik Haraldsson**[1], **Sarah Kefayati**[1], **Chengcheng Zhu**[1], **Sinyeob Ahn**[2], **Gerhard Laub**[2], and **David Saloner**[1,3]

[1]Radiology and Biomedical Imaging, University of California San Francisco, San Francisco, California, United States

[2]Siemens Healthcare, USA

[3]Radiology Service, VA Medical Center, San Francisco, California, United States

Abstract

Object—To evaluate an accelerated 4D flow MRI method that provides a high temporal resolution in a clinically feasible acquisition time for intracranial velocity imaging.

Materials and Methods—Accelerated 4D flow MRI was developed by using a pseudo-random variable-density Cartesian undersampling strategy (CIRCUS) with the combination of k-t, parallel imaging and compressed sensing image reconstruction techniques (k-t SPARSE-SENSE). 4D flow data were acquired on five healthy volunteers and eight patients with intracranial aneurysms using CIRCUS (acceleration factor of R=4, termed CIRCUS4) and GRAPPA (R=2, termed GRAPPA2) as the reference method. Images with three times higher temporal resolution (R=12, CIRCUS12) were also reconstructed from the same acquisition as CIRCUS4. Qualitative and quantitative image assessment was performed on the images acquired with different methods, and complex flow patterns in the aneurysms were identified and compared.

Results—4D flow MRI with CIRCUS was achieved in 5 minutes and allowed further improved temporal resolution of <30 ms. Volunteer studies showed similar qualitative and quantitative evaluation obtained with the proposed approach compared to the reference (overall image scores: GRAPPA2 3.2±0.6, CIRCUS4 3.1±0.7, and CIRCUS12 3.3±0.4; difference of the peak-velocities:

[*]Corresponding author: 185 Berry St, Suite 350, Radiology and Biomedical Imaging, University of California San Francisco, San Francisco, CA 94107, Tel: 415-514-8268, Fax: 415-353-9421, jing.liu@ucsf.edu.

Compliance with Ethical Standards

Conflict of Interest

All authors have no conflict of interest.

Ethical Approval

All procedures performed in studies involving human participants were in accordance with the ethical standards of the institutional and/or national research committee and with the 1964 Helsinki declaration and its later amendments or comparable ethical standards. This study was conducted under IRB approvals (#10-03060) at University of California San Francisco.

Informed Consent

Informed consent was obtained from all individual participants included in the study.

Authors' Contribution

Protocol/project development: Liu, Faraji, Zhu, Ahn, Laub, Saloner
Data collection or management: Liu, Faraji, Haraldsson, Kefayati, Saloner
Data analysis: Liu, Koskas, Faraji, Kao, Wang, Haraldsson, Kefayati, Saloner

−3.83±7.72 cm/s between CIRCUS4 and GRAPPA2, −1.72±8.41 cm/s between CIRCUS12 and GRAPPA2). In patients with intracranial aneurysms, the higher temporal resolution improved capturing of the flow features in intracranial aneurysms (pathline visualization scores: GRAPPA2 2.2±0.2, CIRCUS4 2.5±0.5, and CIRCUS12 2.7±0.6).

Conclusion—The proposed rapid 4D flow MRI with a high temporal resolution is a promising tool for evaluating intracranial aneurysms in a clinically feasible acquisition time.

Keywords

4D flow; acceleration; undersampling; compressed sensing; intracranial; aneurysm

INTRODUCTION

4D flow MR imaging has the ability to provide a comprehensive evaluation of intracranial hemodynamics, which has the potential to provide guidance to clinicians in the evaluation of intracranial aneurysms [1–4], plaque [5,6], arteriovenous malformations [7,8], and cerebral veins [9,10]. Due to the small lumen diameter, intracranial MRI requires a relatively high spatial resolution resulting in long scan times even for limited coverage. High spatiotemporal 4D flow MR imaging is desirable, but the resultant scan times could take 15 minutes or much longer and thus its practical use in clinical studies is limited.

To address this challenge, a variety of acceleration methods have been developed and applied in 4D flow MRI. Non-Cartesian acquisitions such as radial [11–13] and spiral [14–17] sampling trajectories have been investigated for accelerating flow imaging. k-t SENSE and k-t BLAST methods have been used to significantly shorten the scan time in several studies [18,19], but could result in temporal blurring and an underestimation of peak velocities during systole [20–23]. This results from view sharing that is imposed across the temporal domain. Recent work has reported improved performance in this regard by using modified k-t approaches [24,25]. Other approaches that propose the use of compressed sensing (CS) to reduce scan time by exploiting image sparsity [26] have been investigated for accelerating flow imaging [27–31]. CS has been combined with parallel imaging (PI) for further accelerating flow imaging [32–34]. Some of the previous studies were specifically focused on accelerated intracranial 4D flow MRI [22,35,36].

However, limitations in scan time and temporal resolution still remain. Although previous studies have managed to reduce the scan time for intracranial 4D flow imaging to of the order of 10 minutes, this is still lengthy from a clinical perspective. Further reduction in acquisition time will reduce the likelihood of patient motion during the scan, and provide improved patient compliance with studies. The temporal resolution is however commonly sacrificed to obtain an acceptable acquisition time, such as being reduced to around 70 ms or even longer, which in turn can lead to a significant loss of information. Recently it has been suggested that temporal resolution shorter than 40 ms is desirable in 4D flow cardiovascular MRI [37]. In this study, we aim to evaluate the feasibility of performing a highly accelerated 4D flow imaging to shorten the scan time (~5 minutes) as well as to increase the temporal resolution (<30 ms).

CIRcular Cartesian UnderSampling (CIRCUS) [38] is an undersampling strategy that integrates desirable features of randomization, variable-density, and flexible interleaving trajectories on a 3D Cartesian grid. Compared to other undersampling patterns that have been proposed such as the widely-used Poisson-Disk sampling [39–41], CIRCUS provides high computation efficiency, flexible selection of trajectories, and various degrees of randomization, without use of a random operator or lookup table. More importantly, CIRCUS provides flexible interleaving schemes by employing a golden-ratio based profile, which allows for retrospective gating. CIRCUS has first been evaluated by obtaining retrospective undersampling from the fully acquired data [38] and then been implemented and performed prospectively for applications including 3D cardiac CINE MRI and 3D dynamic contrast-enhanced (DCE) MRI [42,43].

In this study, we implemented accelerated 4D flow MRI with CIRCUS acquisition and evaluated it in both healthy volunteers and patients with intracranial aneurysms, by assessing the qualitative and quantitative comparisons to the reference method using GRAPPA [44]. We aim to provide efficient intracranial 4D flow MRI studies that could be completed in a short scan time of ~5 minutes with a high temporal resolution of <30 ms, compared to the conventional acceleration approach with scan times of ~10 minutes with a relatively low temporal resolution of >70 ms.

MATERIALS AND METHODS

Undersampling & Reconstruction

CIRCUS acquisition with spiral-like sampling trajectories [38] was implemented in 4D flow MRI (4-point balanced phase-contrast) by alternating the view ordering during the entire scan with cardiac gating. The same sampling pattern was applied for the phase reference and three velocity encodings. With CIRCUS acquisition, the sampling patterns at different time points during the cardiac cycle were interleaved [42]. Undersampled datasets with CIRCUS acquisition were reconstructed with k-t SPARSE-SENSE [45,46], by using a multi-coil CS reconstruction which exploits joint sparsity along the temporal dimension using a total variation constraint.

The studies were conducted under University of California San Francisco IRB approval and all data were obtained with human subject consent. Both healthy volunteers and patients with intracranial aneurysms were recruited in this study.

Volunteer Study

4D flow data was acquired on a 3.0T MRI scanner (MAGNETOM Skyra, Siemens Medical Solutions, Erlangen, Germany) with a 20-ch head coil. Both the clinical 4D flow imaging protocol with parallel imaging GRAPPA (used as a reference method) and our proposed CIRCUS method were applied on each subject. Prospective gating was applied. Parameters were set to ensure that the number of phases acquired were the maximum achievable within the prospective gating window.

We performed 4D flow MRI acquisitions on 5 healthy subjects (1 female, 31.6±3.6 years) covering the Circle of Willis in the axial view. The scan settings were: VENC=100 cm/s,

FOV=18×18 cm^2, slice thickness=1.4 mm, matrix=128×128×24, FA=15°, TR/TE=6.0/3.5 ms. Clinical 4D flow protocol was applied as the reference, with an acceleration factor of R=2 (effective R=1.6 due to calibration lines acquired around k-space center), a total scan time of 9.9±1.9 minutes (~640 heartbeats), and a temporal resolution of 72 ms (the number of views per segment was 3), termed as GRAPPA2. A shorter scan with the same imaging settings was achieved with CIRCUS acquisition, with an acceleration factor of R=4.0±0.4, a total scan time of 4.1±1.0 minutes (~256 heartbeat), and the regular temporal resolution of 72 ms by choosing the number of segments to be 3, termed CIRCUS4. With CIRCUS acquisition (using the golden-ratio profile), a flexible temporal resolution could be retrospectively selected. In this study, the same data for CIRCUS4 reconstruction were retrospectively reconstructed to provide an increased temporal resolution of 24 ms (R=12.0±1.2, termed CIRCUS12). We then compared the three methods, GRAPPA2, CIRCUS4 and CIRCUS12, by performing both qualitative and quantitative image assessments.

Patient Studies

4D flow MRI with both CIRCUS and GRAPPA acceleration were acquired and compared by assessing the hemodynamics in intracranial aneurysms. We recruited 8 patients with intracranial aneurysms (3 internal carotid artery (ICA), 2 middle cerebral artery (MCA), 1 vertebral artery (VBA), 1 anterior communication artery (ACA), and 1 basilar artery apex (BA) aneurysms). This patient study cohort is a sub-cohort of an ongoing prospective study. Patient demographic information is summarized in Table 1.

Data were acquired on the same scanner as used for the volunteer study with the same head coil, in the view (generally in the coronal plane) covering the vasculature and lesion of interest and providing extended coverage of the feeding arteries. 4D flow sequences were performed following Contrast-Enhanced MR angiography with administration of Gadolinium contrast. The scan settings were: VENC=100cm/s, FOV=24×18cm^2, slice thickness=1.25 mm, matrix=192×144×24-26, FA=6°, and TR/TE=6.1-6.4/3.4-3.7 ms. The reference 4D flow imaging protocol GRAPPA2 (R=1.6) was acquired with a total scan time of 10.4±1.2 minutes (~720 heartbeats) and a temporal resolution of 73-77 ms; CIRCUS4 (R=3.9±0.6) was acquired with a scan time of 5.2±0.8 minutes (~288 heartbeats) and a similar temporal resolution of 73-77 ms; and CIRCUS12 images with a higher temporal resolution of 24-26 ms (R=11.8 ± 2.0) were also retrospectively reconstructed.

Data Processing & Analysis

MRI data were acquired and then transferred to a high performance server for off-line reconstruction. Vessel segmentation, streamline and pathline visualization were performed and generated using an in-house script written in Python and with the commercial flow visualization software ParaView (Kitware Inc., Clifton Park, NY).

The three different methods, GRAPPA2, CIRCUS4 and CIRCUS12, were compared by assessing image quality and performing quantitative measurements on the volunteer studies. The qualitative assessment was conducted by two experienced reviewers blindly on the MR flow imaging. Image quality was assigned using a 5-point scale: 4 = excellent, 3 = slightly

limited but good, 2 = suboptimal, 1 = minimally perceived, and 0 = not perceived: for each of the following flow features:

– magnitude image at peak systolic cardiac phase (artifact level, noise level, vessel depiction)

– velocity image at peak systolic cardiac phase (artifact level, noise level, vessel depiction, and flow pattern)

– phase-contrast MR angiography (PC-MRA) (vessel depiction)

– streamline CINE & at peak systolic cardiac phase (flow patterns)

– pathline CINE (particle trajectories)

A Wilcoxon paired sample signed-rank test was performed on the scores to assess the difference (p-value of 0.05 was used as the significant level).

For volunteer scans covering the Circle of Willis, regions of interest (ROIs) were selected on both left and right middle cerebral arteries. Mean velocities within the ROIs through all time points and mean velocities at peak systole were measured and compared between images from the reference study and those acquired with CIRCUS. The following metrics are reported: the bias and confidence intervals for comparing the quantitative velocity measurements, t-test results, orthogonal regression, and correlation coefficient to assess the difference and correlation of the paired measurements.

For the data acquired on patients with intracranial aneurysms, quantitative comparisons were performed between different methods by evaluating the velocities within the aneurysms and selected ROIs (5 adjacent slices) in the feeding vessels of the aneurysms. Voxel-wise velocities in the aneurysms and mean-velocities in the ROIs were measured and compared between different methods. Streamlines and pathlines were generated and evaluated by comparing the visualization of the complex flow patterns in the aneurysms, using the previously described 5-point scale as described above.

RESULTS

Images were successfully acquired on all subjects and were processed for analysis and comparisons. Figure 1 shows the magnitude and velocity images acquired on a representative volunteer subject, with GRAPPA2, CIRCUS4 and CIRCUS12 (columns) respectively. Despite the significant reduction in scan time (from 9.8 to 4.7 minutes), CIRCUS maintains reasonable image quality even at R=12 (Figure 1, right column, CIRCUS12, temporal resolution=24 ms). This is also demonstrated in PC-MRA maximum intensity projection (MIP) and streamline and pathline visualizations (at the time point of peak velocity) where the flow patterns were clearly captured, as shown in Figure 2.

4D flow images were evaluated based on a series of image features, as described in the Data Analysis Section. Table 2 shows the qualitative image comparisons between GRAPPA and CIRCUS acquisitions on the healthy volunteers. It demonstrates that the accelerated 4D flow method with CIRCUS acquisition provided comparable image quality to the conventional GRAPPA. CIRCUS12 allowed a high temporal resolution of 24 ms with acceleration factor

of R=12 and achieved a slightly higher overall image quality score as reported in Table 2. The Wilcoxon signed rank test showed that the scores for the different methods were not significantly different ($p>0.05$).

The quantitative comparisons of the velocity measurements in MCAs and the corresponding orthogonal regression and Bland-Altman plots are shown in Figure 3. As shown in Table 3, there was no significant difference ($p>0.05$ using paired t-test) in velocity measurements between the methods (CIRCUS4 vs. GRAPPA2, CIRCUS12 vs. GRAPPA2, CIRCUS4 vs. CIRCUS12) and the paired measurements were also shown to be highly correlated ($p<0.05$).

4D flow images obtained in eight patients with aneurysms using GRAPPA2, CIRCUS4 and CIRCUS12 were compared by evaluating the flow patterns (streamlines and pathlines) in the aneurysms. Streamlines were successfully generated in all patient data sets, and pathlines in the aneurysms were obtained in six of the eight patients. For two patients with MCA aneurysms, pathlines were not successfully generated due to slow flow or small aneurysm size. The qualitative scoring on visualization of abnormal flow patterns in the aneurysms for different methods is reported in Table 4. With further reduced scan time and improved temporal resolution, CIRCUS12 provides comparable streamlines (score of 3.1 v.s. 3.2) and improved pathline visualization (2.7 v.s. 2.2), compared to those with GRAPPA2 (Table 4).

Figure 4 shows the aneurysms and the ROIs chosen in the feeding arteries of the aneurysms in patients for quantitative comparisons on the velocities, as reported in Table 5. Although no significant difference was found between the methods in the mean-velocities of the feeding arteries, the variations in the measurements between different methods were found to be larger than those in volunteers. Voxel-wise comparisons of the velocities in the aneurysms showed no significant difference between the different methods (Table 5), while the variations between GRAPPA2 and CIRCUS methods were twice as the ones between CIRCUS4 and CIRCUS12.

In Figures 5–7, streamlines (b) and pathlines (c) (at the time point of peak velocity) from three patients with intracranial arterial aneurysms obtained with different methods are shown; MRA images of the aneurysms are also displayed (a). The streamlines are similar among the different methods, however, overall, CIRCUS could provide improved pathline visualization (better tracking of the swirling flow patterns in the aneurysms as shown in Figures 5&7). It can be seen in Figure 6 that CIRCUS retains pathlines in regions of the aneurysm where there is slow recirculating flow, providing visualization of flow in those locations, which is not the case for GRAPPA2. We also note that for the viewing angle used in Figure 6, the high velocity components in the proximal parent vessel lie behind the slow flow regions and are therefore not visualized on CIRCUS but remain visible on GRAPPA2 as GRAPPA2 fails to display the overlying slow intra-aneurysmal flow. Since variations in the data post-processing such as vessel segmentation, streamline and pathline generations could not be fully avoided, there were visible differences among the generated flow patterns.

DISCUSSION

There is considerable recent interest in 4D flow methods in the MRI research community. This reflects the potentially strong clinical impact that a comprehensive and quantitative assessment of hemodynamics may provide. Evolution of intracranial aneurysmal disease is known to be related to hemodynamic forces acting on the vessel wall. The distribution of Wall Shear Stress (WSS) on the aneurysm wall can be estimated from 4D flow MRI data, and low WSS was shown to be an important contributor to local remodeling of the arterial wall and to aneurysm growth and rupture [47]. However, as stated above, there are challenges in 4D flow MRI that have to be addressed before it attains broad acceptability for its clinical use.

Acquisition time is challenging for 4D flow. Reducing scan time not only permits the practical clinical use of the approach, it also improves patient comfort and reduces healthcare costs. We report here the development and validation of an efficient 5-minute approach. Overall, we were able to demonstrate that the proposed approach provides qualitatively and quantitatively comparable results to those acquired with the conventional method, while the proposed method further reduced the scan time by another factor of 2 and improved the temporal resolution.

Contrast-enhanced MR angiography (CE-MRA) is a routine clinical protocol used to image aneurysms at our institution (to image the geometry and measure size of aneurysms). In our study, 4D flow MRI was applied immediately after the routine contrast-enhanced MRA. As demonstrated in previous studies [48,49], 4D flow MRI is expected to benefit from improved signal-to-noise ratio in magnitude images and noise reduction in velocity maps compared to those without contrast enhancement.

In this study, a routine 4D flow study and an undersampled 4D flow study were added to the routine clinical imaging. This resulted in a total time in the scanner that was difficult for the clinical patients to endure. In order to minimize the total time that they needed to be in the scanner we chose to reduce the total acquisition time by using a lower temporal resolution in this comparison. Although temporal resolution of less than 40 ms remains desirable, as noted in [37], the methods that we used were compared with the same temporal window so the conclusions of their relative performance should not be affected. (We also note, that others have also used temporal resolutions greater than 40 ms [1,2,5].) Establishing adequate performance of our accelerated method will permit us to use better temporal resolution in subsequent studies without incurring an excessively long acquisition time.

A second-order Maxwell correction has been applied in the online reconstruction for the data acquired with GRAPPA2 as provided by the vendor. A second-order polynomial eddy current correction was performed in the off-line postprocessing for the data acquired with GRAPPA2 and CIRCUS. In the current study, our intracranial scans were conducted at iso-center with a small field of view, and thus the phase errors caused by Maxwell terms were expected to be very small, although ideally we should have Maxwell corrections for CIRCUS as well.

Partial volume effect is always challenging for imaging small vessels and in quantitative mapping. Given the small sizes of the intracranial vessels and relatively low spatial resolution that can be achieved using 4D flow MRI, partial volume effects could be an important factor that affects the accuracy of the velocity maps that we have obtained in this study, although image post-processing has been carefully performed (such as vessel segmentation using the contours from MRA). Although our current study focuses on reducing scan time and improving temporal resolution, the acceleration could be exploited for achieving higher spatial resolution, which could help reduce partial volume effects.

Although the differences of the mean velocities between GRAPPA2, CIRCUS4, and CIRCUS12 in both volunteer and patient studies were not significant, we found larger variations in patients than those in volunteers (Table 5 vs Table 3). Patient studies required specification of different imaging orientations and identification of more complex vascular anatomy. Furthermore, patients often have anxiety and other conditions that make it more challenging for them to remain still for a long MRI exam. In comparison, the volunteer study including young healthy subjects and imaging coverage was consistent across subjects resulting in less variation in those measurements. Although the same imaging slab was chosen for GRAPPA2 and CIRCUS during the MRI scan, there was a slight mismatch between the two different acquisitions presumably because of patient movement. Careful registration was applied between the data sets, although potential spatial shifts and partial voxel effect remain given current spatial resolution. Quantitative voxel-wise comparisons were quite sensitive especially for the complex flow patterns in the aneurysms where slow flow, which has an inherently low velocity-to-noise ratio, is prevalent. Although overall our results showed no statistically significant difference between the voxel-wise comparisons between the GRAPPA2 and CIRCUS methods, two of the cases including the case with the smallest aneurysm (size of 3mm) had larger disagreements.

As shown in the Results (Figures 5&7), the pathlines with CIRCUS could provide better tracking of the swirling flow patterns in the aneurysms compared to those with GRAPPA. This is because CIRCUS better accounts for the temporal information continuity, with an interleaved data acquisition through time. In particular, with a higher temporal resolution (24 vs. 73 ms), CIRCUS12 provides finer pathline patterns in the aneurysms due to an improved temporal continuity in the image reconstruction, which improves particle tracing for the pathline generation (as shown in Figures 5–7). The accuracy of the quantitative flow method is crucial for precise diagnosis and consistent monitoring for patients who are being followed longitudinally. Because of acquisition time constraints and relatively smaller flow variations through the cardiac cycle, lower temporal resolution is often used for intracranial imaging. However, this study demonstrates that improved temporal continuity is useful for improving particle tracing in the aneurysms (mainly slow flows). Future studies need to investigate whether the improved temporal resolution could provide improved measurements of the other derived hemodynamic descriptors such as wall shear stress, oscillating shear indices, pressure, and so on.

In addition to reducing the scan time to limit potential motion artifacts that might otherwise occur during a long scan, our proposed method used the CIRCUS scheme that employs a

spiral-like sampling pattern and more frequent acquisition of the center of k-space, which is inherently motion robust and could be very useful for unstable patients.

In addition to the advantages of scan-time reduction and/or higher temporal resolution, accelerated 4D flow MRI also allows for increased options for developing advanced 4D MRI techniques that would otherwise require prohibitively long scan time. This includes multi-VENC [4,50,51] methods, which require more velocity encodings (longer scan time) either to improve the velocity-to-noise ratio (VNR) or to cover a greater range of velocities; higher-directional velocity encoding (ICOSA6) [52], for improved quantification of turbulence and the associated pressure drop; or simply for imaging applications with a higher spatial resolution for better visualization of small vessels or for larger coverage such as in whole brain, chest or abdominal imaging.

The focus of this study is to demonstrate the feasibility of an undersampling approach for reliably acquiring intracranial 4D flow MRI with a reduced scan time and much improved temporal resolution. Although the methods were applied to a group of volunteers and patients, the clinical value of the approach, requires a study with a larger cohort of patients and more quantitative hemodynamic parameters. In this study, we used a conventional 4D flow MRI method with clinically-relevant imaging settings on human subjects in order to validate our proposed method. Future studies will be conducted in a flow phantom with a complex structured velocity field that is not subject to uncontrolled effects during the scan (e.g., movement, or heart-rate variability) and that allows extended scan time where imaging settings can be optimized. For this research project, image reconstruction of the 4D flow images was performed off-line using a high performance server (Four 2.5GHz AMD Opteron 6380 with 256GB Memory). The large computation cost associated with parallel imaging and compressed sensing techniques resulted in image reconstruction times of 2-4 hours in the current study with a CPU-based solver. This needs to be significantly improved if the method is to become clinically viable, which could be accomplished by the use of dedicated GPU-based workstations.

CONCLUSIONS

In summary, we have implemented and validated a highly accelerated 4D flow MRI method for intracranial imaging, which can be completed in 5 minutes with a high temporal resolution of < 30ms. The proposed method has been shown, based on qualitative and quantitative assessment of the images of healthy volunteers as well as patients with intracranial aneurysms, to be comparable to a conventional 4D flow MRI method. This offers the promise of an efficient approach for depicting abnormal flow patterns in intracranial aneurysms.

Acknowledgments

This work was supported in part by grant from the NIH K25EB014914 (JL), R56HL133663 (JL), and R01HL114118 (DS).

References

1. Boussel L, Rayz V, Martin A, Acevedo-Bolton G, Lawton MT, Higashida R, Smith WS, Young WL, Saloner D. Phase-contrast magnetic resonance imaging measurements in intracranial aneurysms in vivo of flow patterns, velocity fields, and wall shear stress: comparison with computational fluid dynamics. Magn Reson Med. 2009; 61:409–417. [PubMed: 19161132]
2. Isoda H, Ohkura Y, Kosugi T, Hirano M, Takeda H, Hiramatsu H, Yamashita S, Takehara Y, Alley MT, Bammer R, Pelc NJ, Namba H, Sakahara H. In vivo hemodynamic analysis of intracranial aneurysms obtained by magnetic resonance fluid dynamics (MRFD) based on time-resolved three-dimensional phase-contrast MRI. Neuroradiology. 2010; 52:921–928. [PubMed: 20012431]
3. Wu C, Schnell S, Vakil P, Honarmand AR, Ansari SA, Carr J, Markl M, Prabhakaran S. In Vivo Assessment of the Impact of Regional Intracranial Atherosclerotic Lesions on Brain Arterial 3D Hemodynamics. AJNR Am J Neuroradiol. 2017; 38:515–522. [PubMed: 28057635]
4. Schnell S, Ansari SA, Wu C, Garcia J, Murphy IG, Rahman OA, Rahsepar AA, Aristova M, Collins JD, Carr JC, Markl M. Accelerated dual-venc 4D flow MRI for neurovascular applications. J Magn Reson Imaging. 2017; 46:102–114. [PubMed: 28152256]
5. Wetzel S, Meckel S, Frydrychowicz A, Bonati L, Radue EW, Scheffler K, Hennig J, Markl M. In vivo assessment and visualization of intracranial arterial hemodynamics with flow-sensitized 4D MR imaging at 3T. AJNR Am J Neuroradiol. 2007; 28:433–438. [PubMed: 17353308]
6. Hope TA, Hope MD, Purcell DD, von Morze C, Vigneron DB, Alley MT, Dillon WP. Evaluation of intracranial stenoses and aneurysms with accelerated 4D flow. Magn Reson Imaging. 2010; 28:41–46. [PubMed: 19577400]
7. Ansari SA, Schnell S, Carroll T, Vakil P, Hurley MC, Wu C, Carr J, Bendok BR, Batjer H, Markl M. Intracranial 4D flow MRI: toward individualized assessment of arteriovenous malformation hemodynamics and treatment-induced changes. AJNR Am J Neuroradiol. 2013; 34:1922–1928. [PubMed: 23639564]
8. Wu C, Ansari SA, Honarmand AR, Vakil P, Hurley MC, Bendok BR, Carr J, Carroll TJ, Markl M. Evaluation of 4D vascular flow and tissue perfusion in cerebral arteriovenous malformations: influence of Spetzler-Martin grade, clinical presentation, and AVM risk factors. AJNR Am J Neuroradiol. 2015; 36:1142–1149. [PubMed: 25721076]
9. Hope MD, Purcell DD, Hope TA, von Morze C, Vigneron DB, Alley MT, Dillon WP. Complete intracranial arterial and venous blood flow evaluation with 4D flow MR imaging. AJNR Am J Neuroradiol. 2009; 30:362–366. [PubMed: 18653687]
10. Schuchardt F, Schroeder L, Anastasopoulos C, Markl M, Bauerle J, Hennemuth A, Drexl J, Valdueza JM, Mader I, Harloff A. In vivo analysis of physiological 3D blood flow of cerebral veins. Eur Radiol. 2015; 25:2371–2380. [PubMed: 25638218]
11. Barger AV, Peters DC, Block WF, Vigen KK, Korosec FR, Grist TM, Mistretta CA. Phase-contrast with interleaved undersampled projections. Magnetic resonance in medicine: official journal of the Society of Magnetic Resonance in Medicine/Society of Magnetic Resonance in Medicine. 2000; 43:503–509.
12. Gu T, Korosec FR, Block WF, Fain SB, Turk Q, Lum D, Zhou Y, Grist TM, Haughton V, Mistretta CA. PC VIPR: a high-speed 3D phase-contrast method for flow quantification and high-resolution angiography. AJNR American journal of neuroradiology. 2005; 26:743–749. [PubMed: 15814915]
13. Johnson KM, Lum DP, Turski PA, Block WF, Mistretta CA, Wieben O. Improved 3D phase contrast MRI with off-resonance corrected dual echo VIPR. Magn Reson Med. 2008; 60:1329–1336. [PubMed: 19025882]
14. Park JB, Olcott EW, Nishimura DG. Rapid measurement of time-averaged blood flow using ungated spiral phase-contrast. Magnetic resonance in medicine: official journal of the Society of Magnetic Resonance in Medicine/Society of Magnetic Resonance in Medicine. 2003; 49:322–328.
15. Sigfridsson A, Petersson S, Carlhall CJ, Ebbers T. Four-dimensional flow MRI using spiral acquisition. Magnetic resonance in medicine : official journal of the Society of Magnetic Resonance in Medicine/Society of Magnetic Resonance in Medicine. 2012; 68:1065–1073.

16. Kadbi M, Negahdar M, Traughber M, Martin P, Amini AA. Assessment of flow and hemodynamics in the carotid artery using a reduced TE 4D flow spiral phase-contrast MRI. Conf Proc IEEE Eng Med Biol Soc. 2013; 2013:1100–1103. [PubMed: 24109884]
17. Dyvorne H, Knight-Greenfield A, Jajamovich G, Besa C, Cui Y, Stalder A, Markl M, Taouli B. Abdominal 4D flow MR imaging in a breath hold: combination of spiral sampling and dynamic compressed sensing for highly accelerated acquisition. Radiology. 2015; 275:245–254. [PubMed: 25325326]
18. Baltes C, Kozerke S, Hansen MS, Pruessmann KP, Tsao J, Boesiger P. Accelerating cine phase-contrast flow measurements using k-t BLAST and k-t SENSE. Magnetic resonance in medicine: official journal of the Society of Magnetic Resonance in Medicine/Society of Magnetic Resonance in Medicine. 2005; 54:1430–1438.
19. Jung B, Stalder AF, Bauer S, Markl M. On the undersampling strategies to accelerate time-resolved 3D imaging using k-t-GRAPPA. Magn Reson Med. 2011; 66:966–975. [PubMed: 21437975]
20. Marshall I. Feasibility of k-t BLAST technique for measuring “seven-dimensional” fluid flow. Journal of magnetic resonance imaging: JMRI. 2006; 23:189–196. [PubMed: 16416437]
21. Stadlbauer A, van der Riet W, Crelier G, Salomonowitz E. Accelerated time-resolved three-dimensional MR velocity mapping of blood flow patterns in the aorta using SENSE and k-t BLAST. European journal of radiology. 2010; 75:e15–21. [PubMed: 19581063]
22. van Ooij P, Guedon A, Marquering HA, Schneiders JJ, Majoie CB, van Bavel E, Nederveen AJ. k-t BLAST and SENSE accelerated time-resolved three-dimensional phase contrast MRI in an intracranial aneurysm. Magma. 2012
23. Carlsson M, Toger J, Kanski M, Bloch KM, Stahlberg F, Heiberg E, Arheden H. Quantification and visualization of cardiovascular 4D velocity mapping accelerated with parallel imaging or k-t BLAST: head to head comparison and validation at 1.5 T and 3 T. J Cardiovasc Magn Reson. 2011; 13:55. [PubMed: 21970399]
24. Schnell S, Markl M, Entezari P, Mahadewia RJ, Semaan E, Stankovic Z, Collins J, Carr J, Jung B. k-t GRAPPA accelerated four-dimensional flow MRI in the aorta: Effect on scan time, image quality, and quantification of flow and wall shear stress. Magn Reson Med. 2013
25. Knobloch V, Boesiger P, Kozerke S. Sparsity transform k-t principal component analysis for accelerating cine three-dimensional flow measurements. Magn Reson Med. 2013; 70:53–63. [PubMed: 22887065]
26. Lustig M, Donoho D, Pauly JM. Sparse MRI: The application of compressed sensing for rapid MR imaging. Magnetic resonance in medicine: official journal of the Society of Magnetic Resonance in Medicine/Society of Magnetic Resonance in Medicine. 2007; 58:1182–1195.
27. Holland DJ, Malioutov DM, Blake A, Sederman AJ, Gladden LF. Reducing data acquisition times in phase-encoded velocity imaging using compressed sensing. Journal of magnetic resonance. 2010; 203:236–246. [PubMed: 20138789]
28. Kwak Y, Nam S, Akcakaya M, Basha TA, Goddu B, Manning WJ, Tarokh V, Nezafat R. Accelerated aortic flow assessment with compressed sensing with and without use of the sparsity of the complex difference image. Magnetic resonance in medicine: official journal of the Society of Magnetic Resonance in Medicine/Society of Magnetic Resonance in Medicine. 2012
29. Zhao F, Noll DC, Nielsen JF, Fessler JA. Separate magnitude and phase regularization via compressed sensing. IEEE transactions on medical imaging. 2012; 31:1713–1723. [PubMed: 22552571]
30. Tao Y, Rilling G, Davies M, Marshall I. Carotid blood flow measurement accelerated by compressed sensing: validation in healthy volunteers. Magn Reson Imaging. 2013; 31:1485–1491. [PubMed: 23830111]
31. Hutter J, Schmitt P, Saake M, Stubinger A, Grimm R, Forman C, Greiser A, Hornegger J, Maier A. Multi-dimensional flow-preserving compressed sensing (MuFloCoS) for time-resolved velocity-encoded phase contrast MRI. IEEE Trans Med Imaging. 2015; 34:400–414. [PubMed: 25252278]
32. Kim D, Dyvorne HA, Otazo R, Feng L, Sodickson DK, Lee VS. Accelerated phase-contrast cine MRI using k-t SPARSE-SENSE. Magnetic resonance in medicine: official journal of the Society of Magnetic Resonance in Medicine/Society of Magnetic Resonance in Medicine. 2012; 67:1054–1064.

33. Hsiao A, Lustig M, Alley MT, Murphy MJ, Vasanawala SS. Evaluation of valvular insufficiency and shunts with parallel-imaging compressed-sensing 4D phase-contrast MR imaging with stereoscopic 3D velocity-fusion volume-rendered visualization. Radiology. 2012; 265:87–95. [PubMed: 22923717]
34. Vasanawala SS, Alley MT, Hargreaves BA, Barth RA, Pauly JM, Lustig M. Improved pediatric MR imaging with compressed sensing. Radiology. 2010; 256:607–616. [PubMed: 20529991]
35. Kecskemeti S, Johnson K, Wu Y, Mistretta C, Turski P, Wieben O. High resolution three-dimensional cine phase contrast MRI of small intracranial aneurysms using a stack of stars k-space trajectory. J Magn Reson Imaging. 2012; 35:518–527. [PubMed: 22095652]
36. Sekine T, Amano Y, Takagi R, Matsumura Y, Murai Y, Kumita S. Feasibility of 4D flow MR imaging of the brain with either Cartesian y-z radial sampling or k-t SENSE: comparison with 4D Flow MR imaging using SENSE. Magn Reson Med Sci. 2014; 13:15–24. [PubMed: 24492737]
37. Dyverfeldt P, Bissell M, Barker AJ, Bolger AF, Carlhall CJ, Ebbers T, Francios CJ, Frydrychowicz A, Geiger J, Giese D, Hope MD, Kilner PJ, Kozerke S, Myerson S, Neubauer S, Wieben O, Markl M. 4D flow cardiovascular magnetic resonance consensus statement. J Cardiovasc Magn Reson. 2015; 17:72. [PubMed: 26257141]
38. Liu J, Saloner D. Accelerated MRI with CIRcular Cartesian UnderSampling (CIRCUS): a variable density Cartesian sampling strategy for compressed sensing and parallel imaging. Quant Imaging Med Surg. 2014; 4:57–67. [PubMed: 24649436]
39. Cook RL. Stochastic Sampling in Computer-Graphics. Acm Transactions on Graphics. 1986; 5:51–72.
40. Dunbar D, Humphreys G. A spatial data structure for fast Poisson-disk sample generation. ACM SIGGRAPH ‘06. 2006:503–508.
41. Vasanawala SS, Murphy MJ, Alley MT, Lai P, Keutzer K, Pauly JM, Lustig M. Practical parallel imaging compressed sensing MRI: Summary of two years of experience in accelerating body MRI of pediatric patients. IEEE International Symposium on Biomedical Imaging: From Nano to Macro. 2011:1039–1043. [PubMed: 24443670]
42. Liu J, Feng L, Shen HW, Zhu C, Wang Y, Mukai K, Brooks GC, Ordovas K, Saloner D. Highly-accelerated self-gated free-breathing 3D cardiac cine MRI: validation in assessment of left ventricular function. Magn Reson Mater Phy. 2017
43. Liu J, Pedoia V, Heilmeier U, Ku E, Su F, Khanna S, Imboden J, Graf J, Link T, Li X. High-temporospatial-resolution dynamic contrast-enhanced (DCE) wrist MRI with variable-density pseudo-random circular Cartesian undersampling (CIRCUS) acquisition: evaluation of perfusion in rheumatoid arthritis patients. NMR Biomed. 2016; 29:15–23. [PubMed: 26608949]
44. Griswold MA, Jakob PM, Heidemann RM, Nittka M, Jellus V, Wang J, Kiefer B, Haase A. Generalized autocalibrating partially parallel acquisitions (GRAPPA). Magnetic resonance in medicine: official journal of the Society of Magnetic Resonance in Medicine/Society of Magnetic Resonance in Medicine. 2002; 47:1202–1210.
45. Otazo R, Kim D, Axel L, Sodickson DK. Combination of compressed sensing and parallel imaging for highly accelerated first-pass cardiac perfusion MRI. Magn Reson Med. 2010; 64:767–776. [PubMed: 20535813]
46. Feng L, Srichai MB, Lim RP, Harrison A, King W, Adluru G, Dibella EV, Sodickson DK, Otazo R, Kim D. Highly accelerated real-time cardiac cine MRI using k-t SPARSE-SENSE. Magn Reson Med. 2013; 70:64–74. [PubMed: 22887290]
47. Boussel L, Rayz V, McCulloch C, Martin A, Acevedo-Bolton G, Lawton M, Higashida R, Smith WS, Young WL, Saloner D. Aneurysm Growth Occurs at Region of Low Wall Shear Stress Patient-Specific Correlation of Hemodynamics and Growth in a Longitudinal Study. Stroke. 2008; 39:2997–3002. [PubMed: 18688012]
48. Bock J, Frydrychowicz A, Stalder AF, Bley TA, Burkhardt H, Hennig J, Markl M. 4D phase contrast MRI at 3 T: effect of standard and blood-pool contrast agents on SNR, PC-MRA, and blood flow visualization. Magn Reson Med. 2010; 63:330–338. [PubMed: 20024953]
49. Hess AT, Bissell MM, Ntusi NA, Lewis AJ, Tunnicliffe EM, Greiser A, Stalder AF, Francis JM, Myerson SG, Neubauer S, Robson MD. Aortic 4D flow: quantification of signal-to-noise ratio as a

function of field strength and contrast enhancement for 1.5T, 3T, and 7T. Magn Reson Med. 2015; 73:1864–1871. [PubMed: 24934930]

50. Nilsson A, Bloch KM, Carlsson M, Heiberg E, Stahlberg F. Variable velocity encoding in a three-dimensional, three-directional phase contrast sequence: Evaluation in phantom and volunteers. Journal of Magnetic Resonance Imaging. 2012; 36:1450–1459. [PubMed: 23065951]
51. Giese, D., Kabbasch, C., Hedderich, D., Maintz, D., Liebig, T., Bunck, A. Hemodynamics in a cerebral aneurysm model treated with different flow diverting stent configurations: Assessment using highly accelerated dual-velocity encoded 3D phase-contrast MRI; Proceedings of the 22nd Annual Meeting of ISMRM; Milan, Italy. 2014. p. 3852
52. Zwart NR, Pipe JG. Multidirectional high-moment encoding in phase contrast MRI. Magnetic Resonance in Medicine. 2013; 69

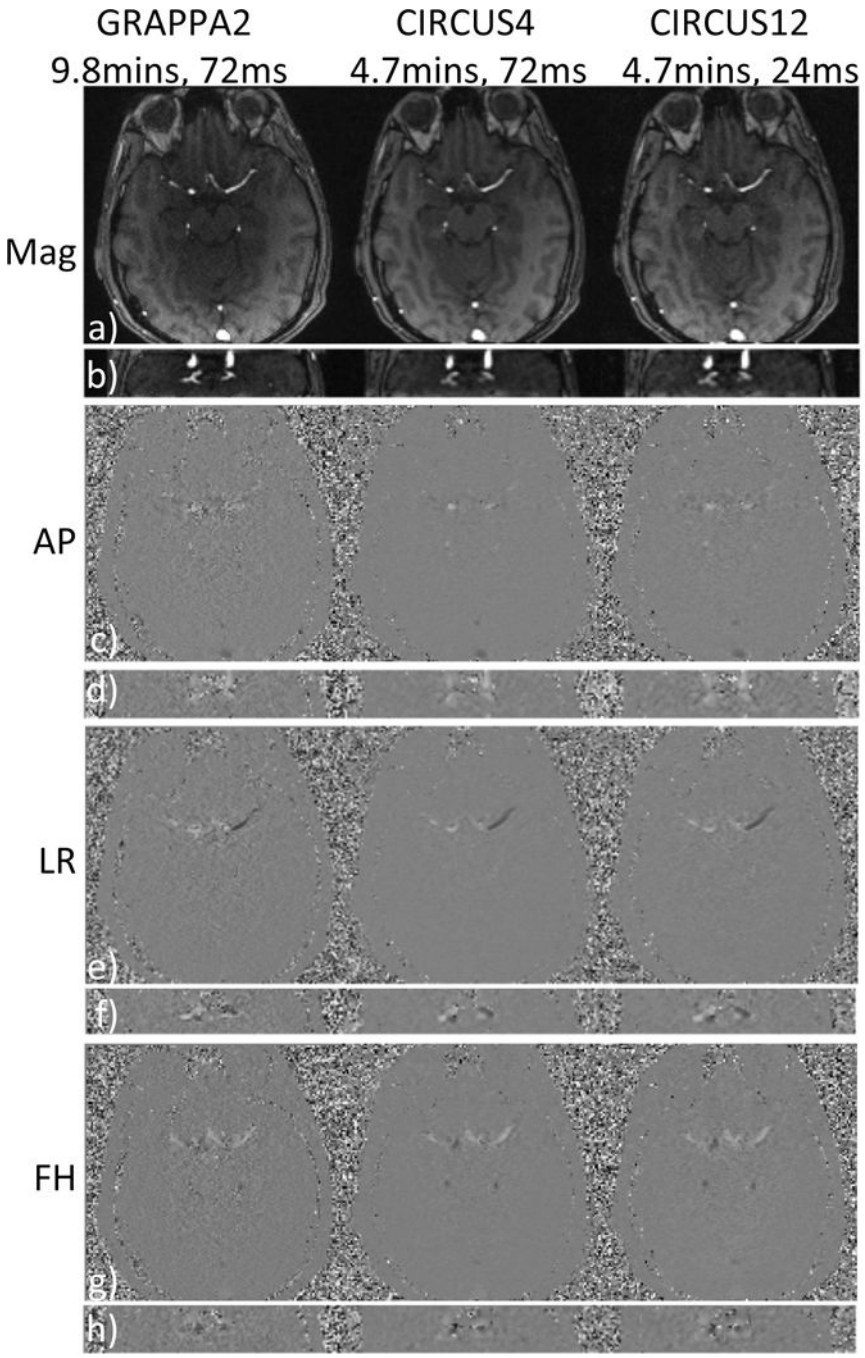

Figure 1.

Magnitude images and three components of velocity (cm/s) acquired with GRAPPA and CIRCUS are shown in two planes (a,c,e&g are in axial view and b,d,f&h are images reformatted in coronal view). AP: anterior-posterior, LR: left-right, FH: foot-head.

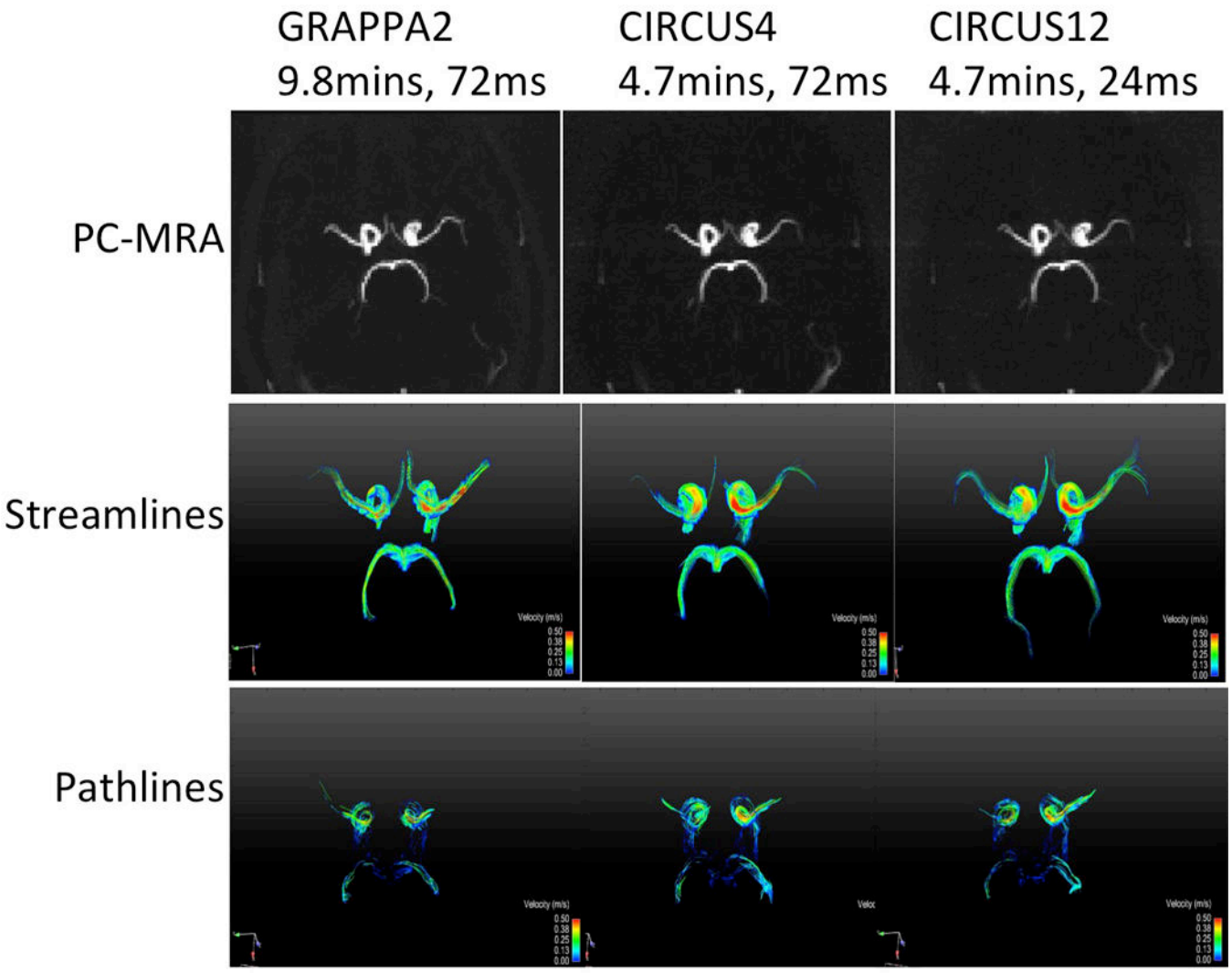

Figure 2.
PC-MRA, streamline and pathline visualizations acquired with GRAPPA and CIRCUS.

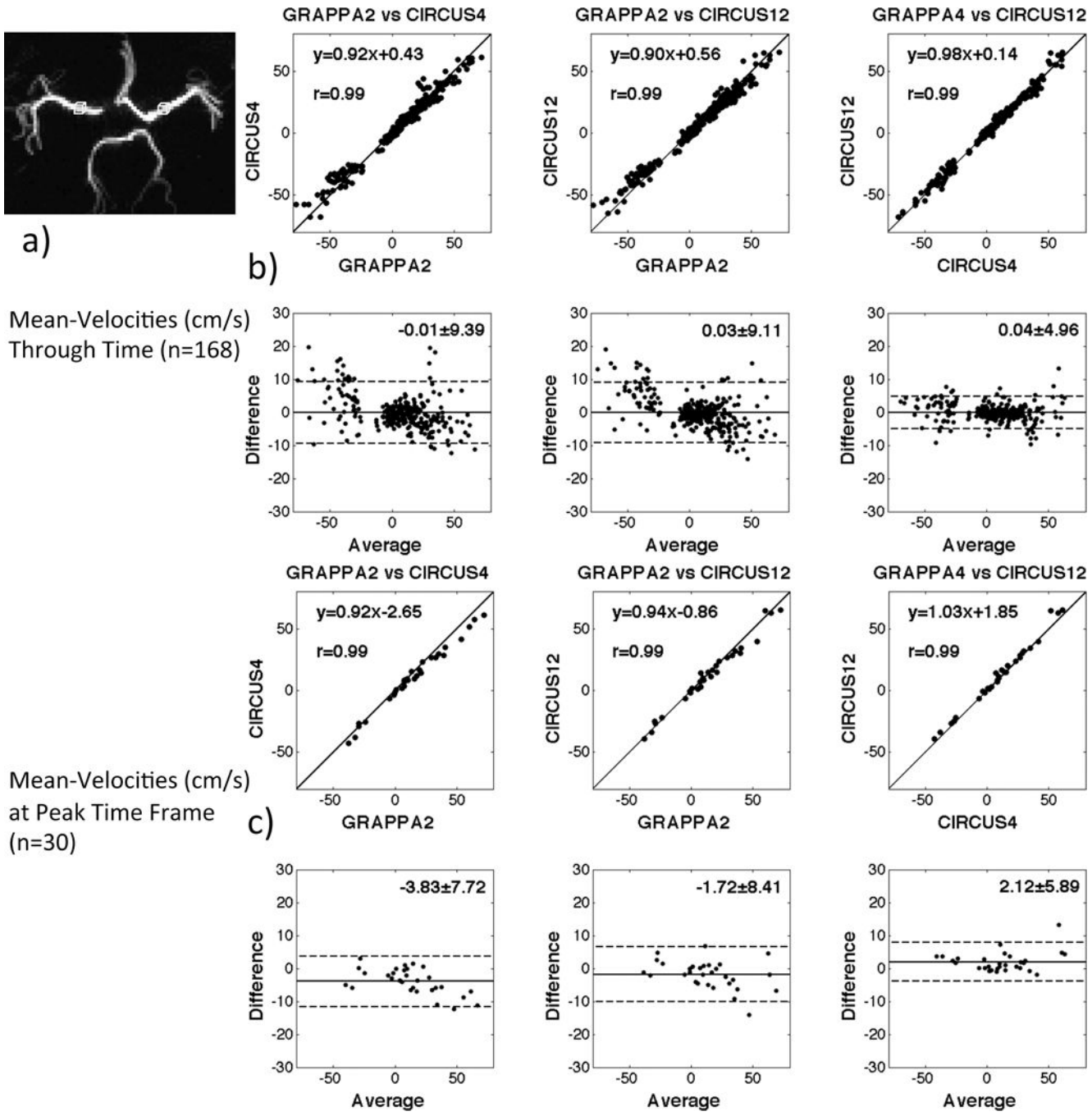

Figure 3.

Orthogonal regression and Bland-Altman plots of the velocity measurements on MCAs obtained with different methods on volunteers. The ROIs selected for measurements are shown as two boxes in a). All measurements shown have unit of cm/s. The difference between the two paired data was showed to be not significant ($p>0.05$).

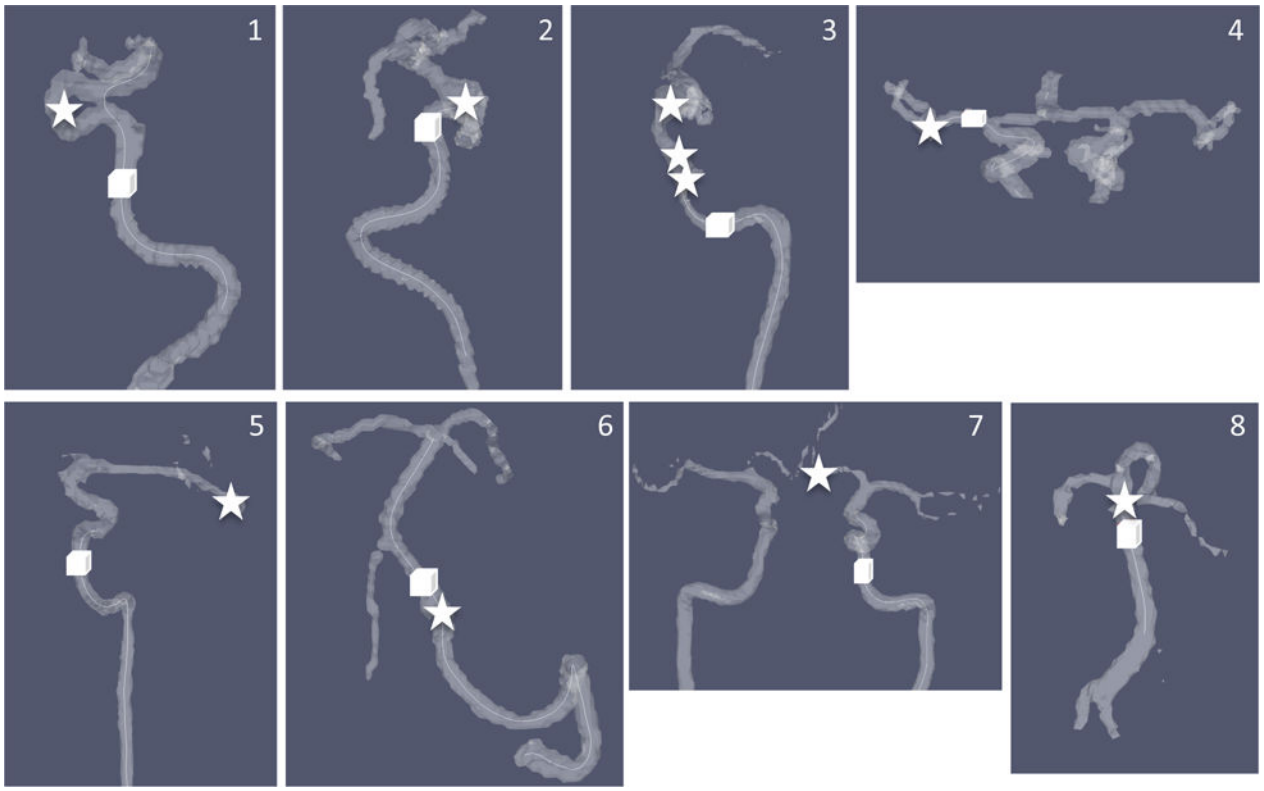

Figure 4.

Locations of the aneurysms (stars) and ROIs selected in their feeding arteries (cubes). Eight cases are corresponding to those listed in Table 1 in the same order. Vessel contours were generated from PC-MRA.

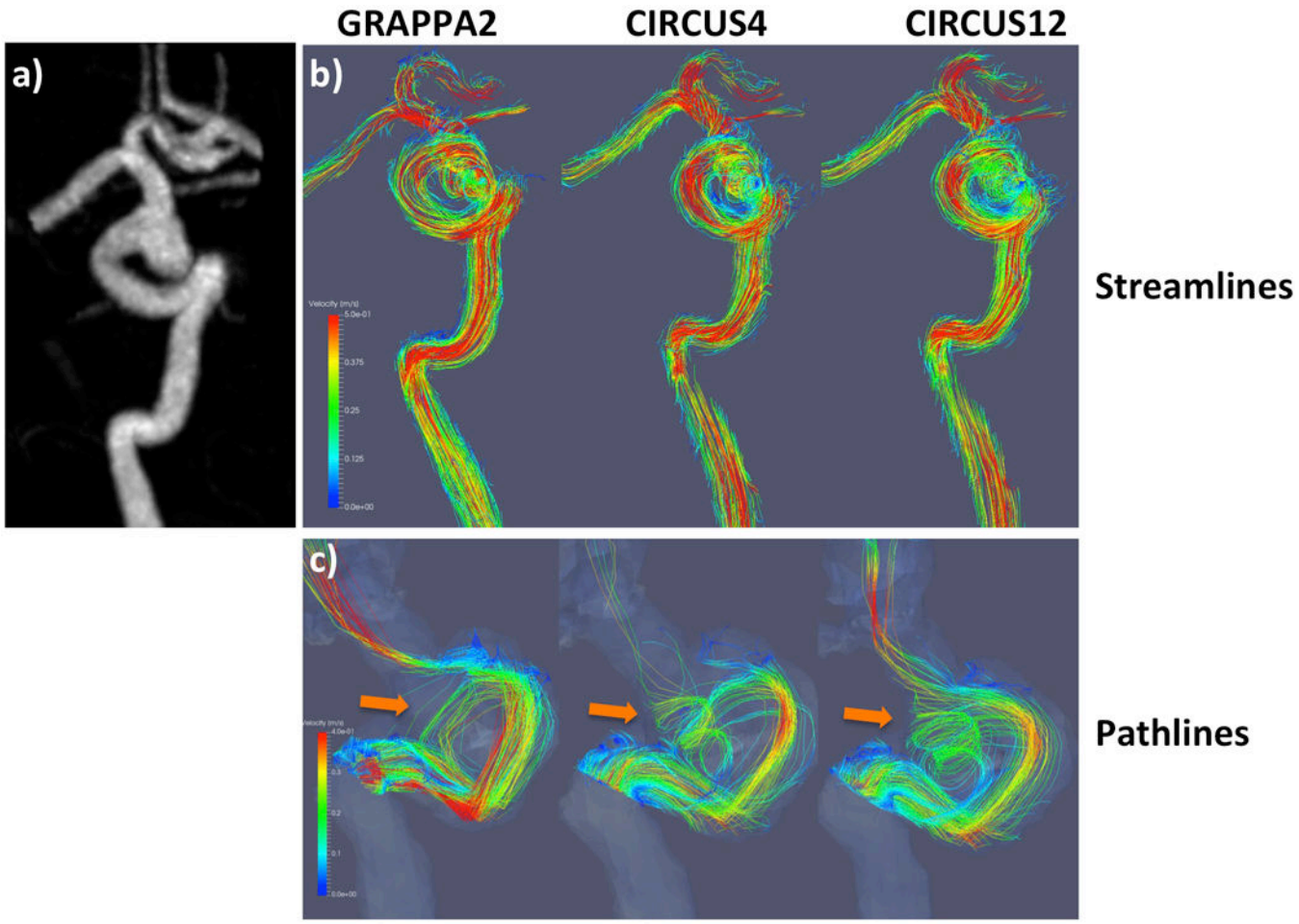

Figure 5.

Streamline (top rows) and pathline (bottom rows) visualizations from a patient with GRAPPA2, CIRCUS4 and CIRCUS12 respectively. This patient had a fusiform aneurysm of the right cavernous and supraclinoid internal carotid artery.

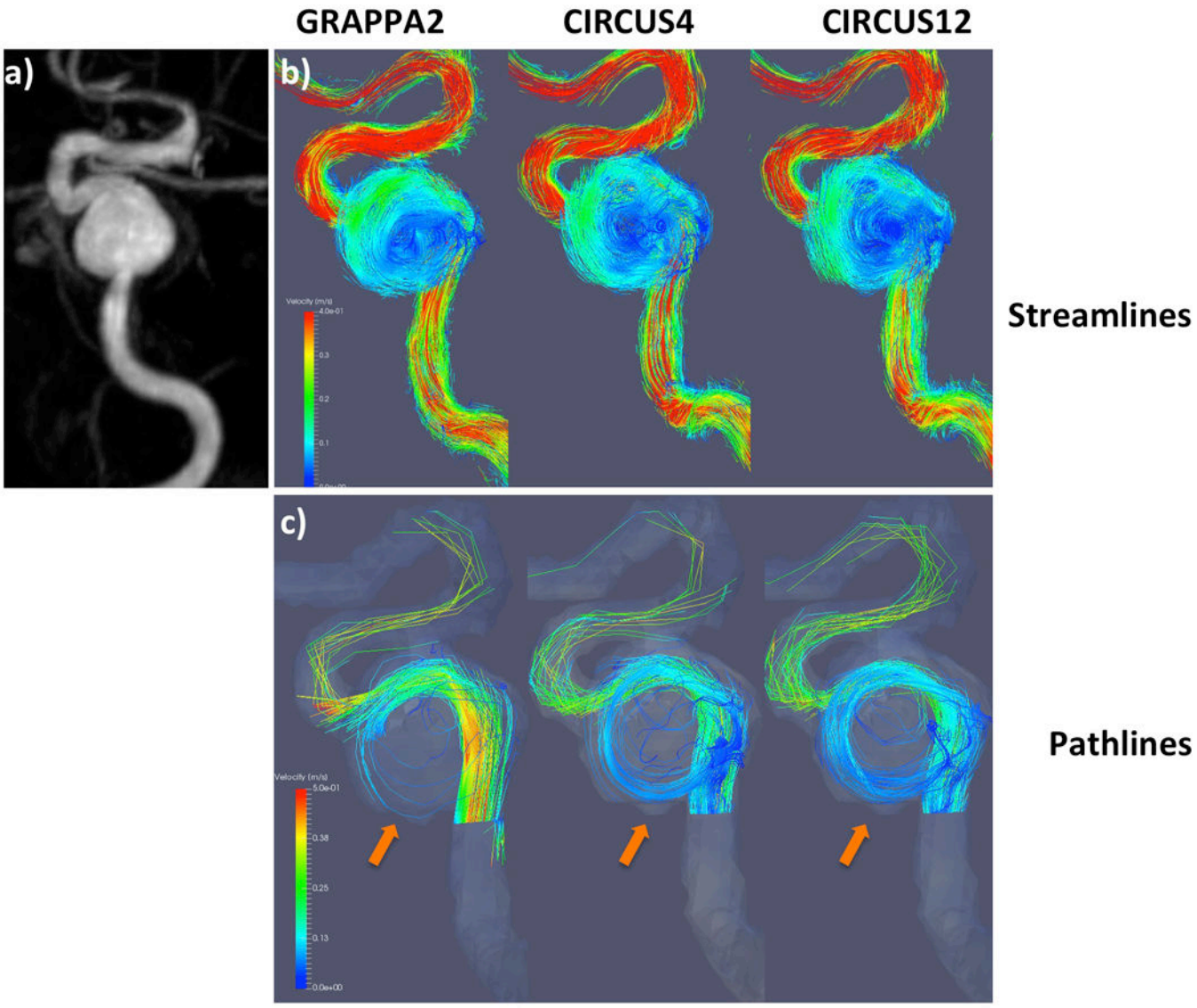

Figure 6.
Streamline (top rows) and pathline (bottom rows) visualizations from a patient with GRAPPA2, CIRCUS4 and CIRCUS12 respectively. This patient was found to have a 14 mm left ICA saccular aneurysm.

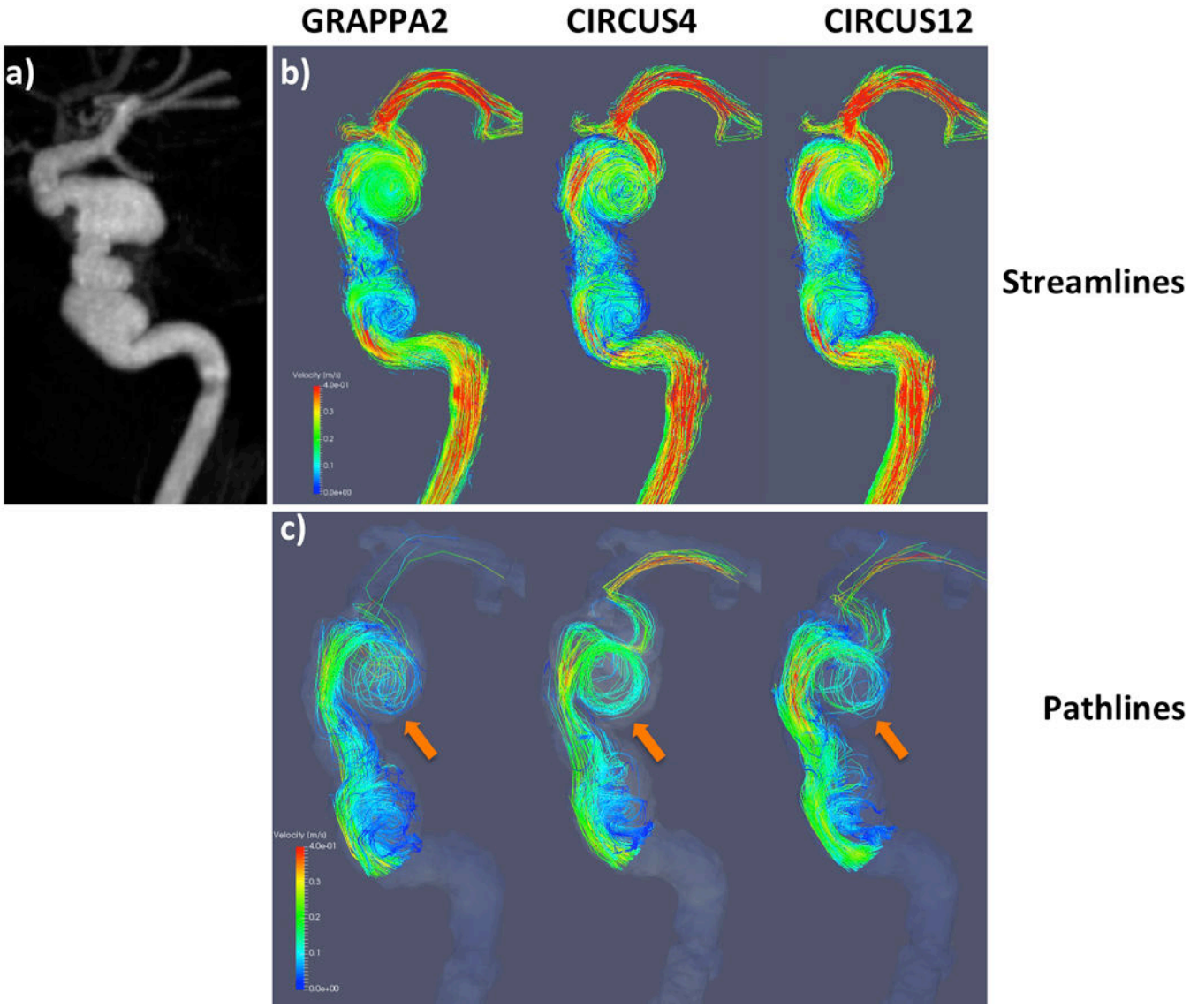

Figure 7.

Streamline (top rows) and pathline (bottom rows) visualizations from a patient with GRAPPA2, CIRCUS4 and CIRCUS12 respectively. This patient was found to have a dysplastic multi-lobed aneurysm involving the right petrous and cavernous ICA, with erosion into the adjacent lateral wall of the sphenoid sinus found incidentally on CTA for headache.

Table 1

Patient demographic data.

Patients	Aneurysm			Age	Sex	HT	DB	SM	HL	CAD	Clinical Presentation
	Location	Shape	Size (mm)								
1	ICA	Saccular	14	70	F	No	No	No	No	No	Asymptomatic
2	ICA	Fusiform	8	52	M	No	No	Yes	No	No	Unrelated stroke
3	ICA	Dysplastic	14	35	M	No	No	No	No	No	Headache
4	L MCA	Saccular	3	77	F	No	No	Yes	No	No	Headache
5	L MCA	Saccular	13	69	M	No	No	Yes	Yes	No	Asymptomatic
6	Vertebral	Dissecting	7	53	M	Yes	Yes	No	No	No	Headache
7	ACA	Saccular	10	67	M	Yes	No	No	Yes	Yes	Asymptomatic
8	Basilar	Saccular	8	84	F	Yes	No	Yes	No	No	Asymptomatic

ICA: internal carotid artery; MCA: middle cerebral artery; ACA: anterior communicating artery; L: left; F: female; M: male; HT: hypertension; DB: diabetes; SM: smoking; HL: Hyperlipidemia; CAD: coronary artery disease.

Table 2

Comparisons of qualitative image quality between images with different acceleration methods applied on volunteers (n=5). The scores from two reviewers between methods were not significantly different on the Wilcoxon signed rank test ($p>0.05$).

Imaging	**GRAPPA2**	**CIRCUS4**	**CIRCUS12**
Scan Time (mins)	9.9±1.9	4.1±1.0	4.1±1.0
Acceleration Factor R	1.6±0	4.0±0.4	12±1.2
Temporal Resolution (ms)	72	72	24
Scores			
Magnitude	3.0±0.4	3.7±0.4	3.2±0.3
Velocity	2.6±0.2	3.6±0.2	3.3±0.4
PC-MRA	3.9±0.2	3.4±0.2	3.1±0.2
Streamline CINE	3.5±0.5	2.9±0.4	3.5±0.4
Streamlines at peak	3.5±0.0	2.2±0.3	3.0±0.6
Pathline CINE	3.0±0.5	3.0±0.6	3.4±0.2
Overall	**3.2**±0.6	**3.1**±0.7	**3.3**±0.4

Table 3

Comparisons of quantitative velocity measurement between images with different acceleration methods applied on volunteers (n=5). (p-value was great than 0.05 for all pairs using paired t-test)

Measurements (cm/s)	**CIRCUS4 v.s. GRAPPA2**	**CIRCUS12 v.s. GRAPPA2**	**CIRCUS4 v.s. CIRCUS12**
	Bias ± 1.96 std		
Mean-Velocities through Time (n=168)	−0.01 ± 9.39 (p=0.988)	0.03 ± 9.11 (p=0.996)	0.04 ± 4.96 (p=0.983)
Mean-Velocities at Peak Time Frame (n=30)	−3.83 ± 7.72 (p=0.81)	−1.72 ± 8.41 (p=0.59)	2.12 ± 5.89 (p=0.76)

Table 4

Evaluation of flow patterns in the aneurysms of patients with different acceleration methods (n=8 for streamlines and n=6 for pathlines). The scores from two reviewers between different methods were not significant on the Wilcoxon signed rank test ($p>0.05$).

Imaging	**GRAPPA2**	**CIRCUS4**	**CIRCUS12**
Scan Time (mins)	10.4±1.2	5.2±0.8	5.2±0.8
Acceleration Factor R	1.6±0	3.9±0.6	11.8±2.0
Temporal Resolution (ms)	73-77	73-77	24-26
Scores			
Streamlines	3.2±0.3	3.1±0.4	3.1±0.4
Pathlines	2.2±0.2	2.5±0.5	2.7±0.6

Table 5

Comparisons of quantitative velocity measurement between images with different acceleration methods applied on patients (n=8). Mean velocities were measured at feeding arteries and voxel-wise velocities within the aneurysms were assessed (locations of the aneurysms and ROIs are shown in Figure 4). (p-value was great than 0.05 for all pairs using paired t-test)

Velocity Measurements Bias ± 1.96 std (cm/s)	CIRCUS4 v.s. GRAPPA2	CIRCUS12 v.s. GRAPPA2	CIRCUS4 v.s. CIRCUS12
Feeding Arteries			
Mean-Velocities through Time (n=246)	1.78±10.59 (p=0.11)	1.49±10.95 (p=0.18)	−0.29±3.65 (p=0.79)
Mean-Velocities at Peak Time Frame (n=24)	1.38±13.84 (p=0.75)	0.65±14.32 (p=0.88)	−0.73±4.42 (p=0.87)
Aneurysms			
Voxel-wise Velocities through Time (n=69312)	−0.02±9.58 (p=0.55)	−0.07±10.35 (p=0.08)	−0.05±5.19 (p=0.18)
Voxel-wise Velocities at Peak Time Frame (n=6504)	−0.03±9.39 (p=0.83)	−0.04±9.88 (p=0.79)	−0.01±5.75 (p=0.94)